

PHYSICOCHEMICAL INVESTIGATION OF ANTI-COVID19 DRUGS USING SEVERAL MEDICINAL PLANTS

FATEMEH MOLLAAMIN *

Department of Biomedical Engineering, Faculty of Engineering and Architecture, Kastamonu University, Kastamonu, Turkey.

ABSTRACT

The goal of this paper was determining the physical and chemical properties of some medicinal plants which are used against the Covid19 symptoms. In this work, seven medicinal species for the most frequently symptoms of Covid19 disease such as fever, cough, sore throat, shortness of breath, anorexia, muscle-joint pain, headache and Nausea-vomiting based on the fidelity level index has been accomplished.

Positive stranded RNA viruses, coronaviruses (CoVs), can infect humans and multiple species of animals through enteric, respiratory, and central nervous system diseases with attractive targets for designing anti- Covid19 conjunction. In this work, it has been investigated the compounds of kaempferol, quercetin, demethoxycurcumine, naringenin, apigenine-7-glucoside, oleuropein and catechin as a probable anti pandemic Covid19 receptor derived from medicinal plants.

Anti-Covid19 through the hydrogen bonding using the physicochemical properties including heat of formation, Gibbs free energy, electronic energy, charge distribution of active parts in the hydrogen bonding, NMR estimation of medicinal ingredients jointed to the database amino acids fragment of Tyr-Met-His as the selective zone of the Covid19, positive frequency and intensity of different normal modes of these structures have been evaluated. The theoretical calculations were done at various levels of theory to gain the more accurate equilibrium geometrical results, and IR spectral data for each of the complex proposed drugs of N-terminal or O-terminal auto-cleavage substrate were individually determined to elucidate the structural flexibility and substrate binding of seven medicinal plants jointed to active site of Covid19 molecule. A comparison of these structures with two configurations provides new insights for the design of substrate-based anti-targeting Covid19. This indicates a feasible model for designing wide-spectrum of anti- Covid19 drugs. The structure-based optimization of these structures has yielded two more efficacious lead compounds, N and O atoms through forming the hydrogen bonding (H-bonding) with potent anti- Covid19.

Finally, two medicinal ingredients of apigenine-7-glucoside and demethoxycurcumine jointed to TMH have directed to a Monte Carlo (MC) simulation. The results strongly suggest that the different data observed in the apigenine-7-glucoside and demethoxycurcumine in the solvent is principally due to basis set functions, induced by a change in polarity of the environment. It is clear that an increase in the dielectric constants enhances the stability of these anti-Covid19 drugs.

Keywords: Covid19, kaempferol, quercetin, demethoxycurcumine, naringenin, apigenine-7-glucoside, oleuropein, catechins.

INTRODUCTION

The SARS-CoV-2 variant: B.1.1.529 was monitored and evaluated by experts of the technical advisory group on SARS-CoV-2 Virus Evolution in 2021. The epidemiological situation in South Africa has been identified by three different peaks in announced cases, the latest of which was predominantly the Delta variant. Then, infections have increased sharply, simultaneously with finding B.1.1.529 variant.

This variant has a grand number of mutations, some of which are worrying. There is an increased risk of reinfection with this variant comparing to other VOCs. So, current SARS-CoV-2 PCR diagnostics can find this variant. Some experiments have shown that for one large PCR test, one of the three target genes is not found and this test can be applied as a sign for this variant, waiting sequencing approval. By this method, this variant has been found at more rapid amounts than previous waves in infection, recommending that this variant might have a growth privilege.

It has been approved that a detrimental change in COVID-19 epidemiology should be determined as a VOC, and the WHO has determined Covid19.

People are reminded to take measures to decrease their risk of COVID-19 consisting of public health and social measures such as wearing masks, hand hygiene, physical distancing, increasing ventilation of inside spaces, preventing crowded spaces, and getting vaccinated [1-3].

As a matter of fact, CoV closely corresponds to intense breathing syndrome CoV (SARS-CoV) which is an epidemic with short period at its living time. SARS-CoV and MERS-CoV relate to the family Coronaviridae's family as enveloped, positive stranded RNA viruses with around 30,000 nucleotides. It has been reported that the global outbreak of a life-threatening typical pneumonia caused about 800 deaths which was world identified as the harsh syndrome CoV (SARS-CoV) [4-8]. Moreover, developed investigations have indicated that the origin of SARS-CoV based on the phylogenetic analysis is mostly likely from bats which are transferred to human aerosols due to intermediate hosts like infectious palm civets by the virus [9-11].

Thus, the animal disease of CoV due to its power of intermediate transition into persons is a threat which has been summarized with the novel MERS-CoV suggesting bats and dromedary camels as the storage for this virus [12-17].

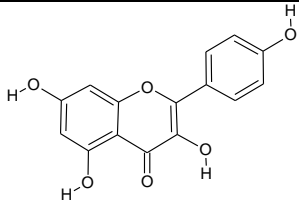
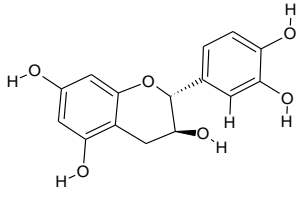
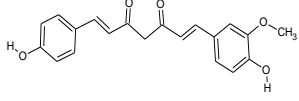
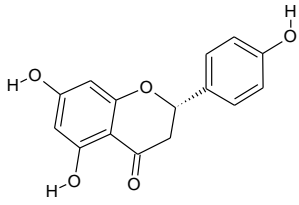
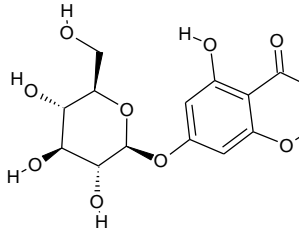
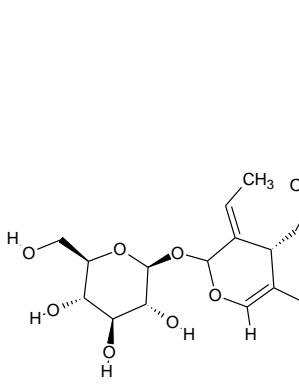
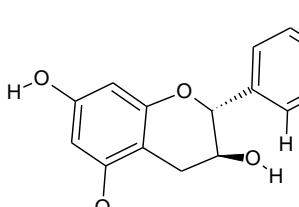
Besides, MERS-CoV declares SARS-like symptoms due to human infections including malaise, rigors, fatigues and high fevers, signs like influenza, but it has been seen later development to a typical pneumonia in most cases [18].

In some researches, it has been discovered that a prototype of the Coronaviridae family is an infectious bronchitis virus (IBV) which relates to the genetic group III of CoV, and causes severe economic defeat for the poultry industry in the world [19-22]. Actually, the scientists have not discovered any vaccine or specific [antiviral treatment](#) ,by management concerning care of symptoms, [supportive treatment](#), and experimental data [23].The results have shown the sample between 1% to 3% [24,25].

Environmental elements can greatly affect the secretion of secondary metabolites from tropical plants. Therefore, great attention has been paid to the secondary metabolites secreted by plants in tropical regions that may be developed as medicines [26-28]. Several compounds, such as flavonoids, from medicinal plants, have been reported to have antiviral bioactivities [29-31]. In the present study, we investigated kaempferol, quercetin, demethoxycurcumine, naringenin, apigenine-7-glucoside, oleuropein and catechin as the probable anti-Covid19 receptor derived from medicinal plants (Table 1).

The findings of the present study will provide other researchers with opportunities to identify the right drug to combat Covid19 using theoretical methods to estimate the impact of hydrogen bonding in different linkage through seven medicinal plants of kaempferol, quercetin, demethoxycurcumine, naringenin, apigenine-7-glucoside, oleuropein and catechin jointed to the active site of Covid19 protein (Fig.1).

Table1. Medicinal ingredients of kaempferol, quercetin, demethoxycurcumine, naringenin, apigenine-7-glucoside, oleuropein and catechin as the probable anti – Covid19 receptor derived from medicinal plants.

| Compound | Molecular structure | Sources |
|-----------------------|---|---|
| Kaempferol |  | Spinach,Cabbage,Dill, Chinese cabbage, Katuk |
| Quercetin |  | Dill, Fennel leaves, Onion, Oregano, Chili pepper |
| Demethoxycurcumine |  | Turmeric, Curcuma |
| Naringenin |  | Citrus fruit |
| Apigenine-7-glucoside |  | Star fruit, Goji berries, Celery, Olive |
| Oleuropein |  | Olive |
| Catechin |  | Green tea |

The findings of the present study will provide other researchers with opportunities to identify the right drug to combat Covid19 using theoretical methods to estimate the impact of hydrogen bonding in different linkage through seven medicinal plants of kaempferol, quercetin, demethoxycurcumine, naringenin, apigenine-7-glucoside, oleuropein and catechin jointed to the active site of Covid19 protein (Fig.1).

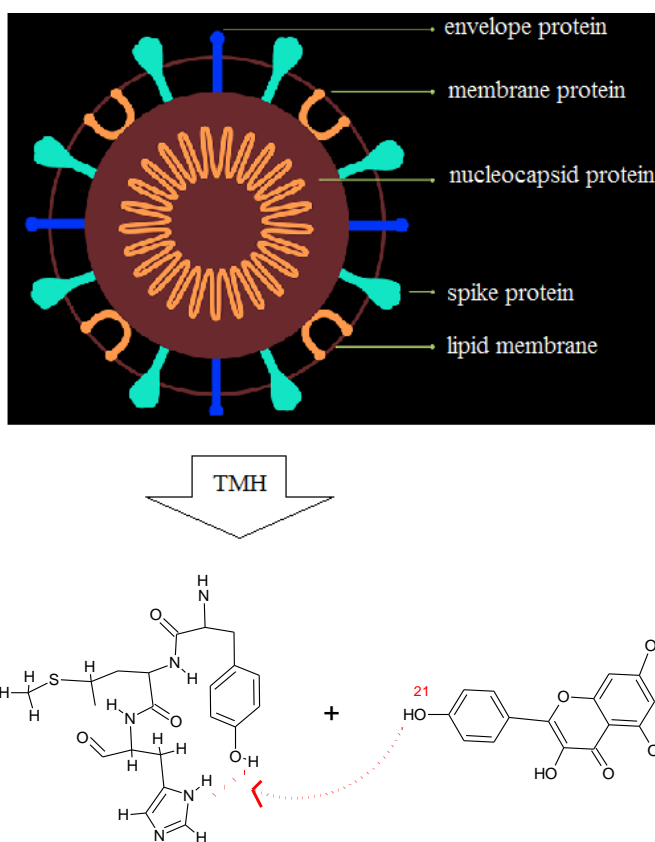


Figure 1. The junction of kaempferol as an anti-Covid19 drug through O21 atom to TMH (Tyr160-Met161-His162) by hydrogen bonding.

MATERIAL AND METHOD

The junction of kaempferol, quercetin, demethoxycurcumine, naringenin, apigenine-7-glucoside, oleuropein and catechin jointed to the active site of Covid19 protein has been accomplished in this work by forming relatively stable complexes through the hydrogen bonding. Thus, a series of quantum theoretical methods of m062x/cc-pvdz pseudo=CEP for complexes of seven inhibitors for Covid19 has been done due to finding the optimized coordination of the best structures of medicinal plant-Tyr160-Met161-His162 drug design model with infrared computations using the Gaussian09 program package [32].

It has been indicated that polarization functions into the applied basis set in the computation always introduce us an important achievement on the modeling and simulation theoretical levels. Normal mode accomplishment is the verdict of harmonic potential wells by analytic methods which maintain the motion of all atoms at the same time in the vibration time scale leading to a natural explanation of molecular vibrations [33-38]. Therefore, the optimized geometry coordination of medicinal ingredients-TMH complexes toward the drug design has been run through the active site of indicated oxygen, nitrogen and hydrogen atoms in the junction of bond and torsion angles (Table 2, Fig.1).

Table 2. Optimized geometry coordination with m062x/cc-pvdz pseudo=CEP pseudo=CEP for kaempferol, demethoxycurcumine, naringenin, apigenine-7-glucoside, and catechins jointed to TMH active site through the drug design method.

| Medicinal ingredients - Covid19 active site | Bond length | (Å) | Bond/Torsion angle | (°) |
|---|-------------|--------|--------------------|----------|
| Kaempferol –TMH | N79-H80 | 10.367 | N79- H80-O21 | 177.056 |
| | H80-O21 | 0.9961 | | |
| | O21-C12 | 13.667 | N79-H80-O21-C12 | 155.865 |
| Demethoxycurcumine-TMH | N91-H92 | 10.316 | N91-H92-O25 | 178.611 |
| | H92-O25 | 0.9955 | | |
| | O25-C6 | 13.714 | N91-H92-O25-C6 | 899.018 |
| Naringenin-TMH | N80-H81 | 10.351 | N80- H81-O20 | 176.623 |
| | H81-O20 | 0.9963 | | |
| | O20-C12 | 13.675 | N80-H81-O20-C12 | -174.489 |
| Apigenine-7-glucoside – TMH | N99-H100 | 10.311 | N99-H100-O20 | 177.402 |
| | H100-O20 | 0.9953 | | |
| | O20-C12 | 13.707 | N99-H100-O20-C12 | -170.878 |
| Catechins – TMH | N83-H84 | 10.314 | N83-H84-O20 | 178.786 |
| | H84-O20 | 0.9955 | | |
| | O20-C12 | 13.697 | N83-H84-O20-C12 | -333.594 |

Therefore, for accomplishing a stable structure of medicinal plant linkage of Covid19 active site, geometry optimization plus the NMR estimation, the frequency and intensity of the vibrational modes were calculated with the quantum mechanical method, and the principal vibrational modes were analyzed by their changes of Gibbs free energy at 300K [39, 40].

Besides, the data has been achieved from thermodynamic parameters of ΔG , ΔH and ΔS for medicinal plant - Covid19 drug design. Thermochemistry analysis follows the frequency and normal mode data. The zero-point energy output in Gaussian-09 has been expanded and corrected as: Thermal correction to energy, thermal correction to enthalpy and thermal correction to the Gibbs free.

In addition the total energies can be calculated as sum of electronic and zero point energies, sum of electronic and thermal energies, sum of electronic and thermal enthalpies and sum of electronic and thermal Gibbs free energies.

The theoretical calculations were done at various levels of theory to gain the more accurate equilibrium geometrical results and IR spectral data for each of the identified compounds. It is supposed that an additional diffuse and polarization functions into the basis set applied in the computation conduct us to the magnificent progress on the results of theoretical methods.

The simulation indicates the approaches which produce a common template of a model at a special temperature by computing all physicochemical properties among the partition function [34].

Each part of the systems including medicinal ingredients-TMH has been optimized using ab-initio via density functional theory including ECP calculations with pseudo=CEP basis sets. In addition, those systems have been evaluated via QM/MM approach through an ONIOM method. In our study, differences of force fields are debated through comparing density and energies with OPLS and AMBER via Monte Carlo optimization. In addition, a Hyperchem professional release 7.01 program has been applied for some additional keywords such as PM3MM, PM6 and pseudo=CEP [41, 42].

Moreover, Monte Carlo simulation (MC) has been accomplished on the anti-Covid19 drugs. This method is a class of computational algorithms that is based on repeated random sampling to estimate the results which is often applied in simulating physical and mathematical systems.

Computation of random or pseudo-random numbers causes the accuracy of calculation especially for unfeasible or impossible to compute an exact result with a deterministic algorithm [43]. It doesn't always need random numbers to use deterministic, pseudo-random sequences, making it easy to test and re-run simulations [44]. The new configuration is accepted if the energy decreases and with a probability of $e^{-\Delta E/KT}$ if the energy increases. This Metropolis procedure ensures that the configurations in the ensemble obey a Boltzmann distribution, and the possibility of accepting higher energy configurations allows MC methods to climb uphill and escape from a local minimum [44].

MC simulations require only the ability to evaluate the energy of the system, which may be advantageous if calculating the first derivative is difficult or time-consuming. Furthermore, since only a single particle is moved in each step, only the energy changes associated with this move must be calculated, not the total energy for the whole system. A disadvantage of MC methods is the lack of the time dimension and atomic velocities, and they are therefore not suitable for studying time-dependent phenomena or properties depending on momentum [44].

RESULTS AND DISCUSSION

NMR calculations on the database of amino acids in beta sheet conformation of Tyr160-Met161-His162 and the two main ingredients of medicinal plants including oleuropein and quercetin have been estimated to unravel the indicated atoms of H, N, O in the active sites of these anti-virus drugs through the formation of hydrogen bonding by indicating the attack zone of TMH (Fig.2 a,b).

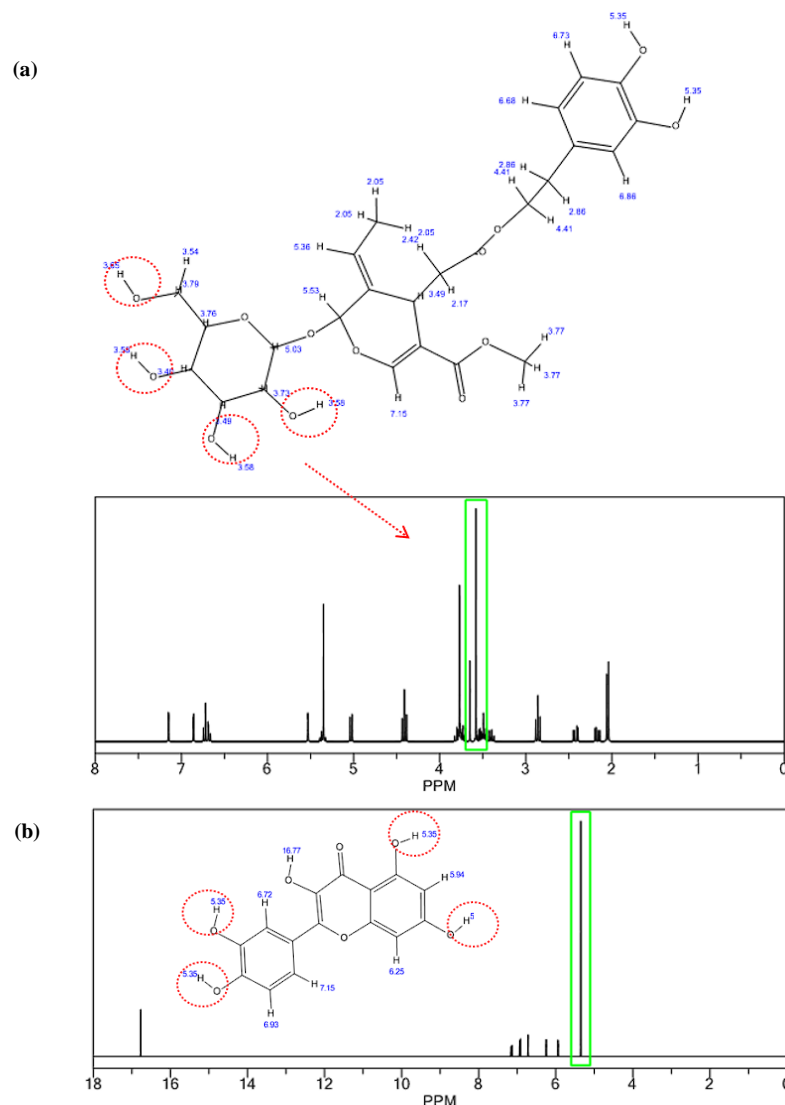


Figure 2. NMR spectra of **a)** oleuropein and **b)** quercetin jointed to TMH Covid19 active site through the drug design method by indicating the active zone of TMH in the drug design process.

The NMR measurements demonstrate the active sites of main ingredients of medicinal species for linking to the Tyr160-Met161-His162 (TMH) in forming the anti-virus drugs while each active atom of oxygen and nitrogen as the electronegative atoms for attaching to the hydrogen denotes the maximal shift in all levels in the NMR spectra (Fig.2 a,b).

Then two main ingredients of medicinal plants including kaempferol and naringenin have been computed for stabilizing the junction of Tyr160-Met161-His162 as the anti- Covid19 through the drug design method using IR spectroscopy using Gaussian09 (Fig.3 a,b).

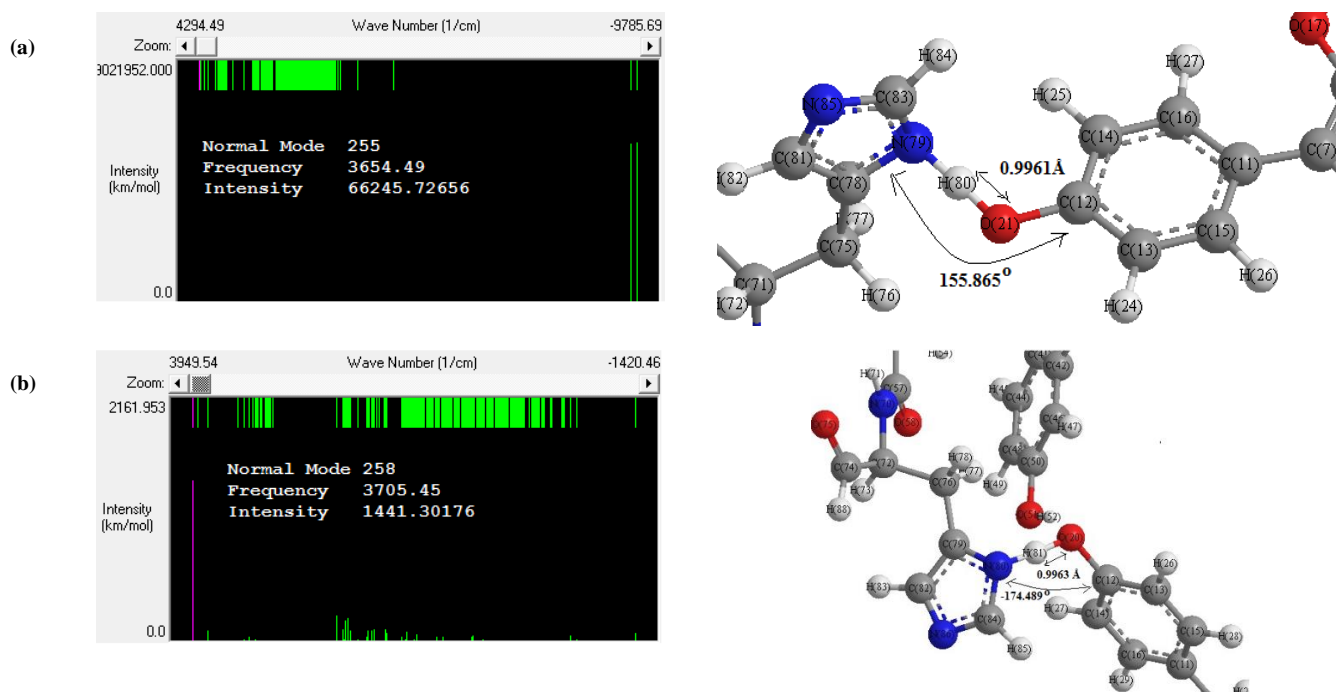


Figure 3. IR spectrum of a) kaempferol and b) naringenin jointed to TMH through the drug design method calculated by m062x/cc-pvdz pseudo=CEP.

Therefore, the thermodynamic properties of ΔG , ΔS , Electronic Energy and Core-Core interaction have determined the stable anti- Covid19 complexes of main ingredients of medicinal species-TMH through the H-bonding formation using the drug design method (Table3 and Fig.4).

Table 3. Physical and thermochemical properties of kaempferol, demethoxycurcumine, naringenin, apigenine-7-glucoside, and catechin jointed to Covid19 active site (TMH) complexes at 300 K.

| Main ingredient - Covid19 active site | $\Delta G \times 10^{-4}$ | ΔS | $E_{\text{electronic}} \times 10^{-4}$ | $E_{\text{core-core}} \times 10^{-4}$ |
|---------------------------------------|---------------------------|--------------|--|---------------------------------------|
| | (kcal/mol) | (kcal/K.mol) | (kcal/mol) | (kcal/mol) |
| Kaempferol | -198.840 | 6.628.135 | -2.171.694 | 1.972.853 |
| Demethoxycurcumine | -208.574 | 6.954.001 | -2.239.025 | 2.030.451 |
| Naringenin | -192.830 | 6.427.278 | -2.110.448 | 1.917.618 |
| Apigenine-7-glucoside | -245.884 | 8.190.807 | -2.979.143 | 2.733.259 |
| Catechin | -200.337 | 6.675.284 | -2.293.383 | 2.093.046 |

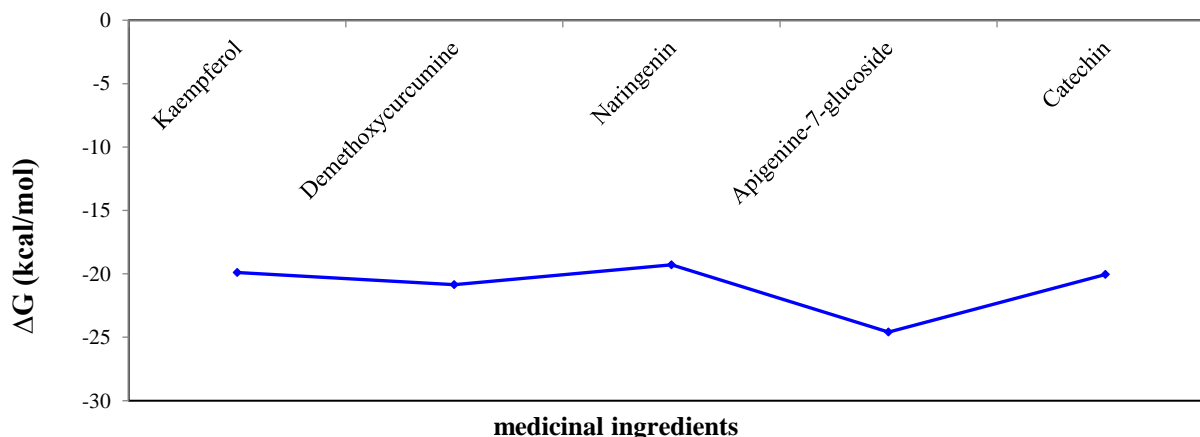
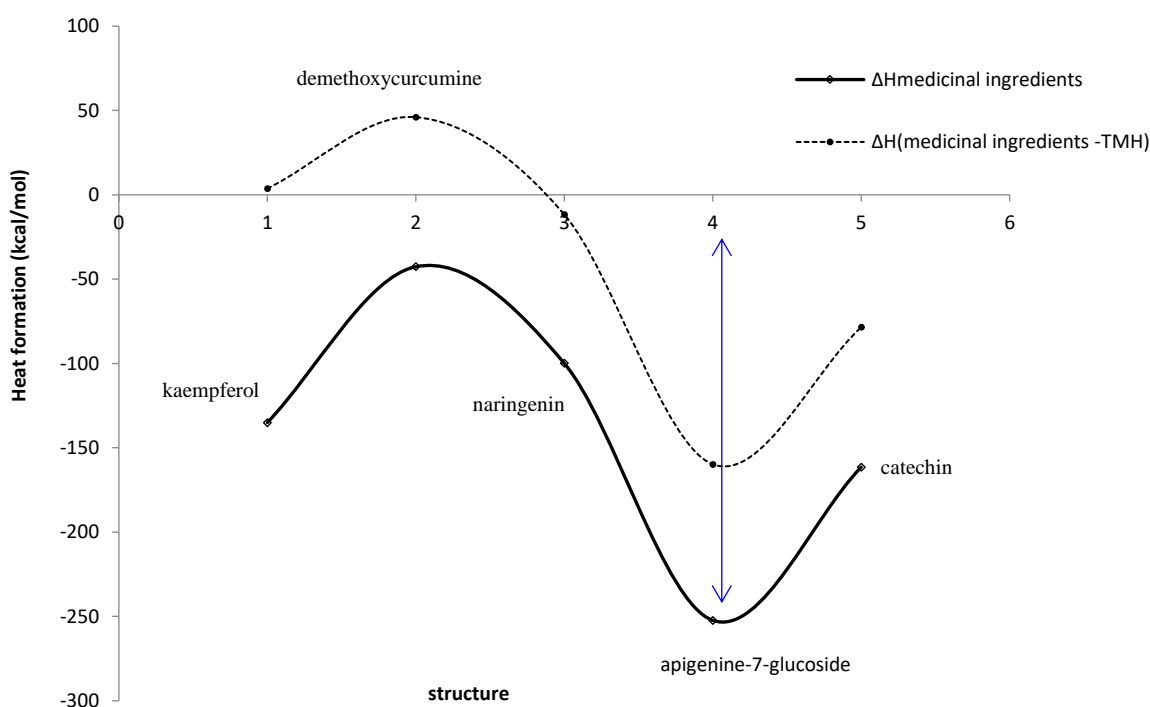


Figure 4. Changes of ΔG for the stable anti- Covid19 complexes of kaempferol, demethoxycurcumine, naringenin, apigenine-7-glucoside, and catechin jointed to TMH through the H-bonding formation using the drug design method.

Moreover, the difference of ΔH_f among kaempferol, demethoxycurcumine, naringenin, apigenine-7-glucoside, and catechin jointed to Covid19 has been discussed the H-bonding due to the database of amino acids in beta sheet conformation; Tyr160-Met161-His162 as the active site of the COVID-19 molecule (Table 4, Fig.5).

Table 4. The Heat of formation, ΔH_F (kcal/mol), among kaempferol, demethoxycurcumin, naringenin, apigenine-7-glucoside and catechin jointed to Covid19 active site (TMH) complexes at 300 K.

| | | | |
|---|---|--|--|
| $\Delta H_{TMH} \times 10^{-4}$ 25.8242 (kcal/mol) | $\Delta H_{\text{Kaempferol}}$ | $\Delta H_{(\text{Kaempferol} \cdot \text{TMH})}$ | $\Delta H_F \times 10^{-4} = \Delta H_{(\text{Kaempferol} \cdot \text{TMH})} - (\Delta H_{\text{Kaempferol}} + \Delta H_{\text{TMH}})$ |
| | -1.350.602 | 37.482 | -258.104 |
| | $\Delta H_{\text{Demethoxycurcumin}}$ | $\Delta H_{(\text{Demethoxycurcumin} \cdot \text{TMH})}$ | $\Delta H_F \times 10^{-4} = \Delta H_{(\text{Demethoxycurcumin} \cdot \text{TMH})} - (\Delta H_{\text{Demethoxycurcumin}} + \Delta H_{\text{TMH}})$ |
| | -426.411 | 460.237 | -258.153 |
| | $\Delta H_{\text{Naringenin}}$ | $\Delta H_{(\text{Naringenin} \cdot \text{TMH})}$ | $\Delta H_F \times 10^{-4} = \Delta H_{(\text{Naringenin} \cdot \text{TMH})} - (\Delta H_{\text{Naringenin}} + \Delta H_{\text{TMH}})$ |
| | -999.081 | -116.632 | -258.154 |
| | $\Delta H_{\text{Apigenine-7-glucoside}}$ | $\Delta H_{(\text{Apigenine-7-glucoside} \cdot \text{TMH})}$ | $\Delta H_F \times 10^{-4} = \Delta H_{(\text{Apigenine-7-glucoside} \cdot \text{TMH})} - (\Delta H_{\text{Apigenine-7-glucoside}} + \Delta H_{\text{TMH}})$ |
| | -2.523.143 | -1.597.850 | -258.149 |
| $\Delta H_{\text{Catechin}}$ | $\Delta H_{(\text{Catechin} \cdot \text{TMH})}$ | $\Delta H_F \times 10^{-4} = \Delta H_{(\text{Catechin} \cdot \text{TMH})} - (\Delta H_{\text{Catechin}} + \Delta H_{\text{TMH}})$ | |
| -1.614.606 | -784.647 | -258.159 | |

**Figure 5.** The difference of ΔH_F among kaempferol, demethoxycurcumin, naringenin, apigenine-7-glucoside, and catechin jointed to Covid19 active site (TMH) complexes at 300 K.

In kaempferol, quercetin demethoxycurcumin, naringenin, apigenine-7-glucoside, oleuropein and catechin jointed to the database of amino acids in beta sheet conformation, Tyr160-Met161-His162, as the active site of Covid19 protein in the process of drug design, the frequency and intensity of various infrared normal modes of medicinal ingredients-TMH complexes have been found to be significantly different through the stability of H-bonding formed between active site of COVID-19 and medicinal ingredients which found the anti- Covid19 (Table 5 & Fig.6).

Table 5. Calculated frequency and intensity of kaempferol, quercetin demethoxycurcumin, naringenin, apigenine-7-glucoside, oleuropein and catechin as anti-Covid19 drugs in different normal modes of infrared spectra.

| Anti-Covid19 drug | Normal mode | Frequency | Intensity | Dipole |
|-----------------------|-------------|-----------|-----------|----------|
| | | (1/cm) | (km/mol) | (Debyes) |
| Kaempferol | 87 | 3765.82 | 1.539.303 | 2.934 |
| Quercetin | 90 | 3765.78 | 1.456.379 | 4.178 |
| Demethoxycurcumin | 123 | 3649.43 | 169.291 | 5.347 |
| Naringenin | 90 | 3650.34 | 141.187 | 3.520 |
| Apigenine-7-glucoside | 147 | 3768.93 | 866.522 | 3.616 |
| Oleuropein | 204 | 3772.69 | 682.212 | 8.522 |
| Catechin | 99 | 3722.79 | 133.225 | 2.400 |

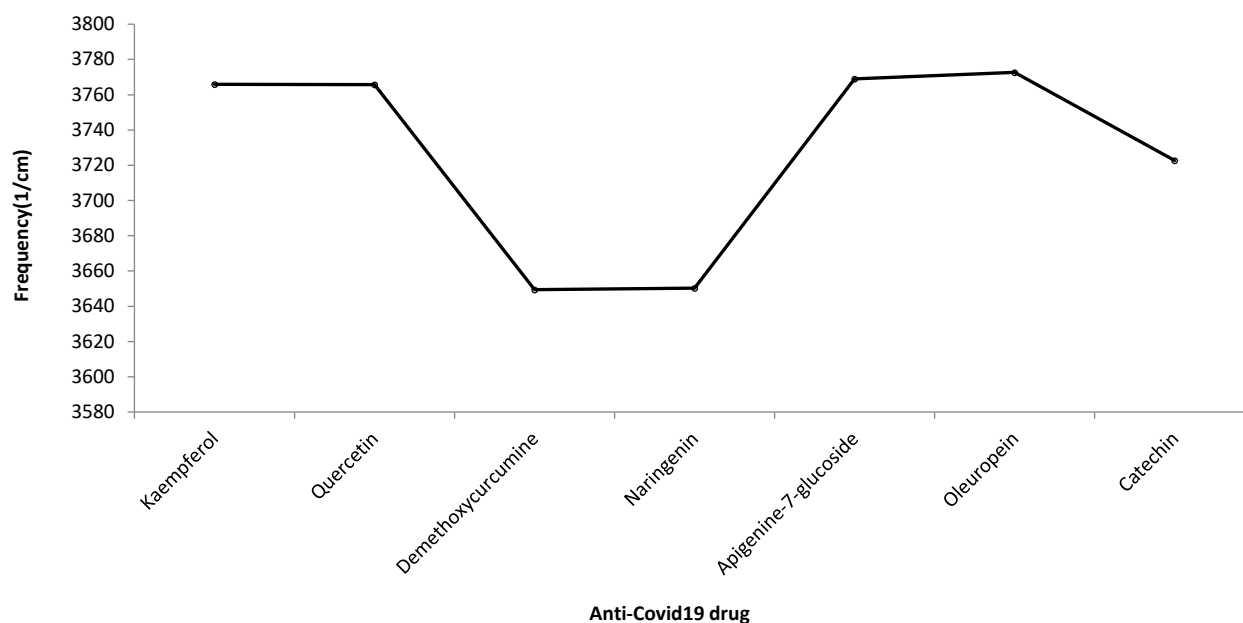


Figure 6. IR spectrum for medicinal plants of kaempferol, quercetin, demethoxycurcumine, naringenin, apigenine-7-glucoside, oleuropein and catechin as anti-Covid19 drugs in different normal modes (Table 5).

The frequency and intensity TMH-junction were found to be significantly different with each medicinal ingredient treatment including kaempferol, quercetin demethoxycurcumine, naringenin, apigenine-7-glucoside, oleuropein and catechin.

It has been seen that by increasing the activity of atoms in the active site of medicinal ingredients, the frequency and intensity of medicinal ingredients-Tyr160-Met161-His162 junction also have increased from 3649.43 to 3765.82 1/cm (demethoxycurcumine/kaempferol) and from 6.82212 to 16.9291 km/mol (oleuropein/ demethoxycurcumine), respectively, with forming hydrogen bonding (Table 5 & Fig.6).

Although we have little information about the interaction of medicinal drugs with Covid19, database amino acids fragment of Tyr160-Met161-His162 as the selective zone of the COVID-19 molecule were found to induce frequency and intensity of spectra.

In the next step, the atomic charge of indicated atoms of oxygen junction of kaempferol, quercetin, naringenin, oleuropein, demethoxycurcumine, apigenine-7-glucoside, and catechin with Tyr160-Met161-His162 have been evaluated in the zone of H-bonding formation (Table 6).

Table 6. The values of atomic charge for labeled oxygen atoms in the attachment of kaempferol, quercetin, naringenin, oleuropein, demethoxycurcumine, apigenine-7-glucoside, and catechins with Tyr160-Met161-His162.

| Kaempferol | charge | Quercetin | charge | Naringenin | charge | Oleuropein | charge |
|--------------------|---------|-----------------------|---------|------------|---------|------------|---------|
| O9 | -0.0778 | O9 | -0.0758 | O9 | -0.1846 | O8 | -0.3197 |
| O17 | -0.2046 | O17 | -0.2097 | O17 | -0.2226 | O9 | -0.3288 |
| O18 | -0.2224 | O18 | -0.2218 | O18 | -0.1917 | O10 | -0.2619 |
| O19 | -0.1821 | O19 | -0.1823 | O19 | -0.3132 | O16 | -0.2164 |
| O20 | -0.3305 | O20 | -0.3299 | O20 | -0.2296 | O18 | -0.4192 |
| O21 | -0.2327 | O21 | -0.2303 | | | O19 | -0.2427 |
| | | O25 | -0.2473 | | | O26 | -0.2572 |
| | | | | | | O35 | -0.2324 |
| | | | | | | O36 | -0.2504 |
| Demethoxycurcumine | charge | Apigenine-7-glucoside | charge | Catechin | charge | | |
| O10 | -0.2979 | O9 | -0.0975 | O9 | -0.1790 | | |
| O13 | -0.2952 | O17 | -0.1846 | O17 | -0.3148 | | |
| O22 | -0.1927 | O18 | -0.1841 | O18 | -0.2275 | | |
| O24 | -0.2396 | O19 | -0.3368 | O19 | -0.2312 | | |
| O25 | -0.2267 | O20 | -0.2243 | O20 | -0.2133 | | |
| | | O22 | -0.2310 | O21 | -0.2130 | | |
| | | O28 | -0.3197 | | | | |
| | | O29 | -0.3255 | | | | |
| | | O30 | -0.3250 | | | | |
| | | O31 | -0.3149 | | | | |

Then, in Fig.7, it has been plotted the changes of atomic charge for labeled oxygen atoms through optimized kaempferol, quercetin, naringenin, oleuropein, demethoxycurcumine, apigenine-7-glucoside, and catechin with Tyr160-Met161-His162 complexes due to formation of H-bonding; so, the results of table 6 in a polar zone have declared the stability of Covid19 drugs which have been modeled using the drug design method .

The largest fluctuation in Fig.7 has been seen for the samples of oleuropein/apigenine-7-glucoside-Tyr160-Met161-His162 considering the oxygen as the electronegative atoms in formation the H-bonding through using the drug design method which has suggested the modeling of anti- Covid19.

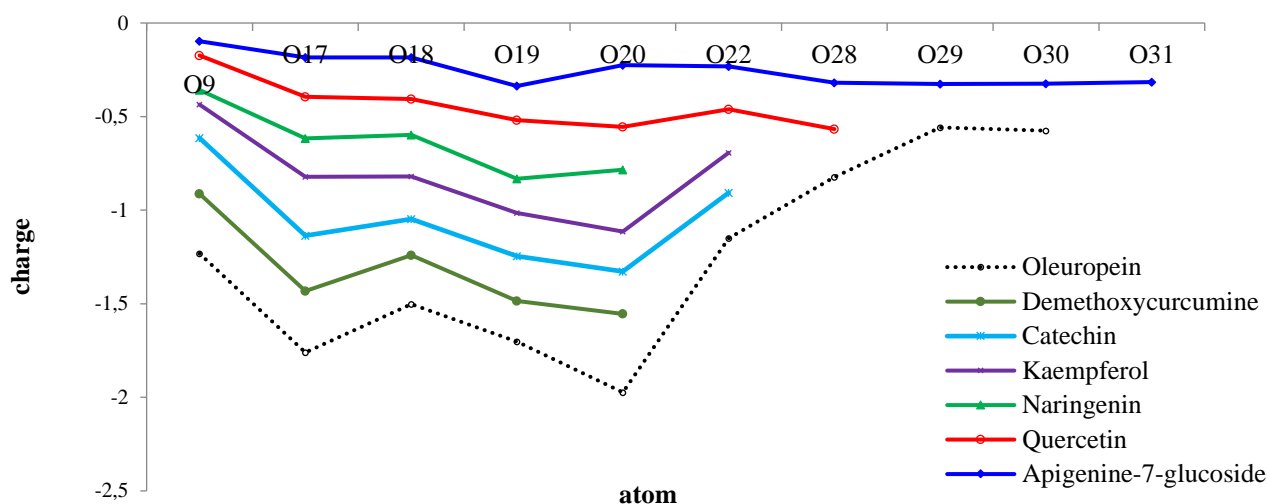


Figure 7. Comparison of atomic charge versus labeled of oxygen atoms in the junction of active sites of kaempferol, quercetin, naringenin, oleuropein, demethoxycurcumine, apigenine-7-glucoside, and catechin with Tyr160-Met161-His162.

Thus the perspective of Fig.7 has proposed the reason for existing observed various results of the atomic charge on medicinal plant- Covid19 complexes as the anti- COVID-19 drugs which are principally related to the position of active sites of indicated oxygen, nitrogen and hydrogen atoms in the junction of bond angles. In fact, the spin density and partial charges have been obtained by fitting the electrostatic potential to fix the charge of oxygen and nitrogen with high electronegativity in junction of electrophilic group of hydrogen in the structures of medicinal plant- Covid19 as the anti-virus drugs which conduct us toward the industry of drug design.

Then, apigenine-7-glucoside and demethoxycurcumine jointed to TMH have directed to a Monte Carlo (MC) simulation by potential energy in 300K energy via time scale (0-100) with max delta and time steps of 0.05 Å, 1, respectively (Fig.8a,b). Optimal values are close to 0.5. Differencing the step size can have a large influence on the acceptance ratio. The MC options dialog box lets us arrange the MC simulation parameters with 100 steps.

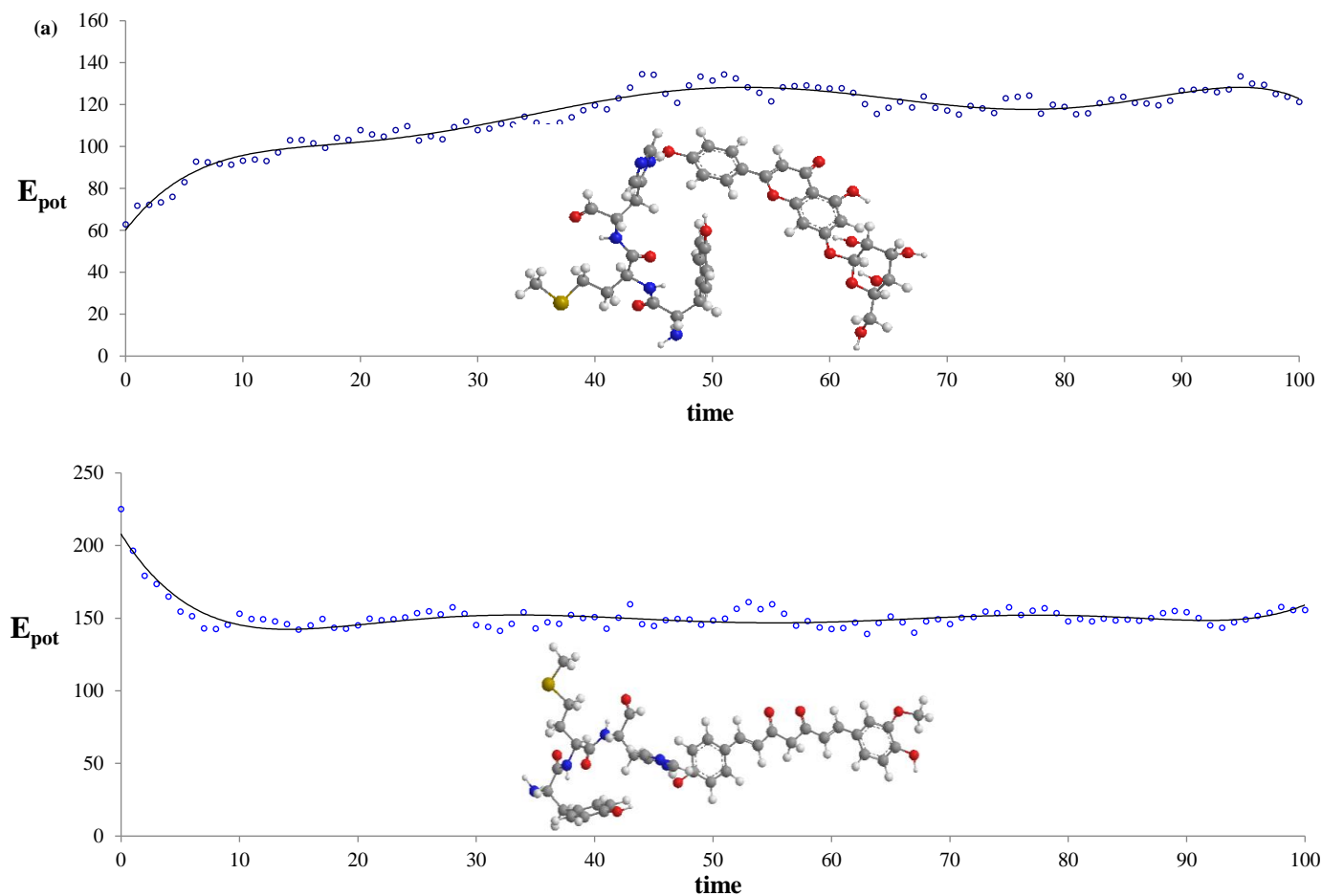


Figure 8. Monte Carlo simulation of **a)** apigenine-7-glucoside **b)** demethoxycurcumine jointed to TMH as the anti-Covid19 drugs.

Study of the solution state has invoked much interest among investigators and a lot has been done in the study of solute-solvent interactions. Water is the main solvent environment for a majority of biomolecules. It has been estimated the potential of apigenine-7-glucoside and demethoxycurcumin with a simulated model of solute-solvent in a periodic box with maximum number of water molecules, minimum distance between solvent and solute molecules using program package HyperChem 8 [45-49].

It has been shown the potential energy graph of apigenine-7-glucoside and demethoxycurcumin in solvent via time scale (0-100) in 300 K using MC method (Max delta =0.05 Å, time steps=1).

The results of the above observations strongly suggest that the different data observed in the apigenine-7-glucoside and demethoxycurcumin in the solvent is predominantly due to basis set functions, induced by a change in polarity of the environment. It is clear that an increase in the dielectric constants increases the stability of these anti-Covid19 drugs.

CONCLUSION

Medicinal plants of kaempferol, quercetin, demethoxycurcumin, naringenin, apigenine-7-glucoside, oleuropein and catechin are capable to join the database amino acids fragment of Tyr160-Met161-His162 as the selective zone of the Covid19 through indicating the shift in their frequency and intensity spectra after estimation by NMR method which are affected by the atomic configuration of the anti-virus.

The stability of H-bonding between several medicinal ingredients of kaempferol, quercetin, demethoxycurcumin, naringenin, apigenine-7-glucoside, oleuropein and catechin and Covid19 through the formation anti-Covid19 through two probabilities of

N⁻⁻⁻⁻H and O⁻⁻⁻⁻H with different atomic charges have been investigated using IR methods. So, the thermodynamic properties of Gibbs free energy, enthalpy of formation, Electronic Energy, Core-Core interaction have approved the stability of anti-Covid19 due to H-bonding formation using the drug design method.

The simulations of medicinal ingredients-Covid19 show that the stabilization energy has been affected by the Monte Carlo force field and different temperature and the best results have been gained for potential energy vs. temperature at MC force field and by increasing of temperature, our calculations have demonstrated that such extrapolation schemes significantly overestimate the medicinal ingredients-Covid19 by active site of molecule (N and O linkage) which are the most active point at indicated structure.

ACKNOWLEDGMENTS

In successfully completing this paper and the research behind it, the authors are grateful to Kastamonu University for their support through the library, the laboratory, and scientific websites.

REFERENCES

- Zhang, J.; Zhou, L.; Yang, Y.; Peng, W.; Wang, W.; Chen, X. [Therapeutic and triage strategies for 2019 novel coronavirus disease in fever clinics.](#) *Lancet* **2020**, 395, e39. [https://doi.org/10.1016/S0140-6736\(20\)30313-5](https://doi.org/10.1016/S0140-6736(20)30313-5).
- Pandey, U.; Greninger, A.L.; Levin, G.R. Pathogen or bystander: clinical significance of detecting human herpesvirus 6 in pediatric cerebrospinal fluid. *J Clin Microbiol* **2020**, 58, e00313-e00320. <https://doi.org/10.1128/JCM.00313-20>.
- Mollaamin, F.; Esmkhani, R.; Monajjemi, M. Mutations in Novel COVID-19 Make it More Dangerous: Prevention Via Scientific Approaches. *Biointerface Res. Appl. Chem* **2021**, 11(3), 10546-10558. <https://doi.org/10.33263/BRIAC113.1054610558>.
- Yan, B.; Chu, H.; Yang, D.; Sze, K.-H.; Lai, P.-M.; Yuan, S.; Shuai, H.; Wang, Y.; Kao, R.Y.-T.; Chan, J.F.-W.; Yuen, K.-Y. Characterization of the Lipid Profile of Human Coronavirus-Infected Cells: Implications for Lipid Metabolism Remodeling upon Coronavirus Replication. *Viruses* **2019**, 11, 73. <https://doi.org/10.3390/v11010073>.
- Fouchier, R. A.M.; Kuiken, T.; Schutten, M.; van Amerongen, G.; van Doornum, G.J.J.; van den Hoogen, B.G.; Peiris, M.; Lim, W.; Stohr, K.; and Osterhaus, A.D.M.E. Aetiology: Koch's postulates fulfilled for SARS virus. *Nature* **2003**, 423, 240. <https://doi.org/10.1038/423240a>.

- Ksiazek, T. G.; Erdman, D.; Goldsmith, C. S.; Zaki, S. R.; Peret, T.; Emery, S.; Tong, S.; Urbani, C.; Comer, J.A.; Lim, W.; Rollin, P.E.; Dowell, S.F.; Ling, A.E.; Humphrey, C.D.; Shieh, W.J.; Guarner, J.; Paddock, C.D.; Rota, P.; Fields, B.; DeRisi, J.; Yang, J.Y.; Cox, N.; Hughes, J.M.; LeDuc, J.W.; Bellini, W.J.; and Anderson, L.J. A novel coronavirus associated with severe acute respiratory syndrome. *N. Engl. J. Med* **2003**, 348, 1953-1966. <https://doi.org/10.1056/NEJMoa030781>.
- Shi, C.S.; Nabar, N.R.; Huang, N.N.; et al. SARS-Coronavirus Open reading frame-8b triggers intracellular stress pathways and activates NLRP3 inflammasomes. *Cell Death Discov.* **2019**, 5:101. <https://doi.org/10.1038/s41420-019-0181-7>.
- Mollaamin, F. Function of Anti-CoV Structure Using INH [1-6]- Tyr160-Met161-His162 Complex. *Biointerface Res. Appl. Chem* **2021**, 11(6), 14433 - 14450. <https://doi.org/10.33263/BRIAC116.1443314450>.
- Mitton, B.; Ruel, R.; Said, M. [Laboratory evaluation of the BioFire FilmArray Pneumonia plus panel compared to conventional methods for the identification of bacteria in lower respiratory tract specimens: a prospective cross-sectional study from South Africa.](#) *Diagn Microbiol Infect Dis* **2021**, 99, 115236. <https://doi.org/10.1016/j.diagmicrobio.2020.115236>.
- Kao, C.-C.; Chiang, H.-T.; Chen, C.-Y.; Hung, C.-T.; Chen, Y.-C.; Su, L.-H.; Shi, Z.-Y. et al. National bundle care program implementation to reduce ventilator-associated pneumonia in intensive care units in Taiwan. *J Microbiol Immunol Infect* **2019**, 52, 592-597. <https://doi.org/10.1016/j.jmii.2017.11.001>.
- Yen, M.Y.; Schwartz, J.; Chen, S.Y.; King, C.C.; Yang, G.Y.; Hsueh, P.R. [Interrupting COVID-19 transmission by implementing enhanced traffic control bundling: Implications for global prevention and control efforts.](#) *J Microbiol Immunol Infect* **2020**, 53, 377-380. <https://doi.org/10.1016/j.jmii.2020.03.011>.
- Álvarez-Lerma, F.; Sánchez García, M.; The multimodal approach for ventilator-associated pneumonia prevention-requirements for nationwide implementation. *Ann Transl Med* **2018**, 6, 420. <https://doi.org/10.21037/atm.2018.08.40>.
- Camélena, F.; Moy, A.C.; Dudoignon, E.; Poncin, T.; Deniau, B.; Guillemet, L.; Le Goff, J. et al. *Diagn Microbiol Infect Dis* **2021**, 99, 115183. <https://doi.org/10.1016/j.diagmicrobio.2020.115183>.
- Dien Bard, J.; McElvania, E. [Panels and Syndromic Testing in Clinical Microbiology.](#) *Clin Lab Med* **2020**, 40, 393-420. <https://doi.org/10.1016/j.cll.2020.08.001>.
- Van, T.T.; Kim, T.H.; Butler-Wu, S.M. Evaluation of the Biofire FilmArray meningitis/encephalitis assay for the detection of Cryptococcus neoformans/gattii. *Clin Microbiol Infect* **2020**, S1198-743X, 30031-30038. <https://doi.org/10.1016/j.cmi.2020.01.007>.
- Tansarli, G.S.; Chapin, K.C. Diagnostic test accuracy of the BioFire(R) FilmArray(R) meningitis/encephalitis panel: a systematic review and meta-analysis. *Clin Microbiol Infect* **2020**, 26, 281-290. <https://doi.org/10.1016/j.cmi.2019.11.016>.
- Nabower, A.M.; Miller, S.; Biewen, B. Association of the FilmArray meningitis/encephalitis panel with clinical management. *Hosp Pediatr* **2019**, 9, 763-769. <https://doi.org/10.1542/hpeds.2019-0064>.
- Cailleaux, M.; Pilmis, B.; Mizrahi, A. Impact of a multiplex PCR assay (FilmArray(R)) on the management of patients with suspected central nervous system infections. *Eur J Clin Microbiol Infect Dis* **2020**, 39, 293-297. <https://doi.org/10.1007/s10096-019-03724-7>.
- She, R.C.; Bender, J.M. Advances in rapid molecular blood culture diagnostics: healthcare impact, laboratory implications, and multiplex technologies. *J Appl Lab Med* **2019**, 3, 617-630. <https://doi.org/10.1373/jalm.2018.027409>.
- Juttukonda, L.J.; Katz, S.; Gillon, J. Impact of a rapid blood culture diagnostic test in a children's hospital depends on Gram-positive versus Gram-negative organism and day versus night shift. *J Clin Microbiol* **2020**, 58, e01400-e01419. <https://doi.org/10.1128/JCM.01400-19>.
- Bakhshi, K.; Mollaamin, F.; Monajjemi, M. Exchange and Correlation Effect of Hydrogen Chemisorption on Nano V(100) Surface: A DFT Study by Generalized Gradient Approximation (GGA). *Journal of Computational and Theoretical Nanoscience* **2011**, 8, 763-768. <https://doi.org/10.1166/jctn.2011.1750>.
- Blauwkamp, T.A.; Thair, S.; Rosen, M.J. Analytical and clinical validation of a microbial cell-free DNA sequencing test for infectious disease. *Nat Microbiol* **2019**, 4, 663-674. <https://doi.org/10.1038/s41564-018-0349-6>.
- Hagen, A.; Eichinger, A.; Meyer-Buehn, M. Comparison of antibiotic and acyclovir usage before and after the implementation of an on-site FilmArray meningitis/encephalitis panel in an academic tertiary pediatric hospital: a retrospective observational study. *BMC Pediatr* **2020**, 20, 56. <https://doi.org/10.1186/s12887-020-1944-2>.

24. Najafloo, N.; Monajjemi, M.; Attarkhasraghi, N.; Kandemirli, F.; Mollaamin, F. The Specification of Observed COVID-19 in England: A Review of Auto-Mutation. *Biointerface Res. Appl. Chem* **2021**, *11*(6), 14794 – 14808. <https://doi.org/10.33263/BRIAC116.1479414808>.
25. Lee, S.H.; Ruan, S.Y.; Pan, S.C.; Lee, T.F.; Chien, J.Y.; Hsueh P.R. Performance of a multiplex PCR pneumonia panel for the identification of respiratory pathogens and the main determinants of resistance from the lower respiratory tract specimens of adult patients in intensive care units. *J Microbiol Immunol Infect* **2019**, *52*, 920-928. <https://doi.org/10.1016/j.jmii.2019.10.009>.
26. G. Guerriero, G. *et al.*, Production of plant secondary metabolites: Examples, tips and suggestions for biotechnologists. *Genes (Basel)*. **2018**, *9*(6) 34-46. <https://doi.org/10.3390/genes9060309>.
27. Yang, L.; Wen, K. S.; Ruan, X.; Zhao, Y.X.; Wei, F. and Wang, Q. Response of plant secondary metabolites to environmental factors, *Molecules* **2018**, *23* (4), 1-26. <https://doi.org/10.3390/molecules23040762>.
28. Zadeh, MAA.; Lari, H.; Kharghanian, L.; Balali, E.; Khadivi, R.; Yahyaei, H.; Mollaamin, F.; Monajjemi, M. Density Functional Theory Study and Anti-Cancer Properties of Shyshaq Plant: In View Point of Nano Biotechnology. *J Comput Theor Nanosci* **2015**, *12*, 4358-4367. <https://doi.org/10.1166/jctn.2015.4366>.
29. Zakaryan, H.; Arabyan, E.; Oo, A.; Zandi, K. Flavonoids: promising natural compounds against viral infections. *Arch. Virol.* **2017**, *162* (9), 2539-2551. <https://doi.org/10.1007/s00705-017-3417-y>.
30. Seema, T.M.; Thyagarajan, S.P. Pa-9: A flavonoid extracted from plectranthus amboinicus inhibits HIV-1 protease. *Int. J. Pharmacogn. Phytochem. Res.* **2016**, *8*(6), 1020-1024.
31. Jo, S.; Kim, S.; Shin, D.H., Kim, M.S. Inhibition of SARS-CoV 3CL protease by flavonoids. *J. Enzyme Inhib. Med. Chem.* **2020**, *35*(1), 145-151, <https://doi.org/10.1080/14756366.2019.1690480>.
32. Akbulut, S. Medicinal Plants Preferences for the Treatment of COVID-19 Symptoms in Central and Eastern Anatolia, Kastamonu Univ., *Journal of Forestry Faculty*, **2021**, *21*(3): 196-207. <https://doi.org/10.17475/kastorman.1048372>.
33. Frisch, M.J.; Trucks, G.W.; Schlegel, H.B.; Scuseria, G.E.; Robb, M.A.; Cheeseman, J.R.; Scalmani, G.; *et al.* *Gaussian 09, Revision B.01.* **2010**. Gaussian Inc., Wallingford.
34. Mollaamin, F.; Monajjemi, M. Harmonic Linear Combination and Normal Mode Analysis of Semiconductor Nanotubes Vibrations. *J. Comput. Theor. Nanosci* **2015**, *12*, 1030-1039. <https://doi.org/10.1166/jctn.2015.3846>.
35. Roy, T. K.; Kopysov, V.; Pereverzev, A.; Šebek, J.; Gerber, R. B.; Boyarkin, O. V. Intrinsic structure of pentapeptide Leu-enkephalin geometry optimization and validation by comparison of VSCF-PT2 calculations with cold ion spectroscopy. *Phys. Chem. Chem. Phys.* **2018**, *20*, 24894-24901. <https://doi.org/10.1039/c8cp03989e>.
36. Ni, W.; Li, G.; Zhao, J.; Cui, J.; Wang, R.; Gao, Z.; Liu, Y. Use of Monte Carlo simulation to evaluate the efficacy of tigecycline and minocycline for the treatment of pneumonia due to carbapenemase-producing *Klebsiella pneumoniae*. *Infect Dis (Lond)* **2018**, *50*, 507-513. <https://doi.org/10.1080/23744235.2018.1423703>.
37. Kawczak, P.; Bober, L.; Bączek, T. QSAR analysis of selected antimicrobial structures belonging to nitro-derivatives of heterocyclic compounds. *Lett Drug Des Discov* **2018c**, *17*, 214-225 <https://doi.org/10.2174/1570180815666181004112947>.
38. McArdle, S.; Mayorov, A.; Shan, X.; Benjamin, S.; Yuan, X. Digital quantum simulation of molecular vibrations. *Chem. Sci.* **2019**, *10*, 5725-5735. <https://doi.org/10.1039/C9SC01313j>.
39. Monajjemi, M.; Mahdavian, L.; Mollaamin, F.; Khaleghian, M. Interaction of Na, Mg, Al, Si with carbon nanotube (CNT): NMR and IR study. *Russ. J. Inorg. Chem* **2009**, *54*, 1465-1473. <https://doi.org/10.1134/S0036023609090216>.
40. Lee, V.S.; Nimmanpipug, P.; Mollaamin, F.; Kungwan, N.; Thanasanvorakun, S.; Monajjemi, M. Investigation of single wall carbon nanotubes electrical properties and normal mode analysis: Dielectric effects. *Russian Journal of Physical Chemistry A* **2009**, *83*, 2288-2296, <https://doi.org/10.1134/S0036024409130184>.
41. Wang, S. Efficiently Calculating Anharmonic Frequencies of Molecular Vibration by Molecular Dynamics Trajectory Analysis. *ACS Omega* **2019**, *4*, 9271- 9283. <https://doi.org/10.1021/acsomega.8b03364>.
42. Monajjemi, M.; Mollaamin, F.; Gholami, M.R.; Yoosbhashizadeh, H.; Sadrnezhad, S.K.; Passdar H. Quantum chemical parameters of some organic corrosion inhibitors, pyridine, 2-picoline 4-picoline and 2,4-lutidine, adsorption at aluminum surface in hydrochloric and nitric acids and comparison between two acidic media. *Main Group Met. Chem.* **2003**, *26*, 349-361. <https://doi.org/10.1515/MGMC.2003.26.6.349>.
43. Ni, W.; Li, G.; Zhao, J.; Cui, J.; Wang, R.; Gao, Z.; Liu, Y. Use of Monte Carlo simulation to evaluate the efficacy of tigecycline and minocycline for the treatment of pneumonia due to carbapenemase-producing *Klebsiella pneumoniae*. *Infect Dis (Lond)* **2018**, *50*(7), 507-513, <http://doi.org/10.1080/23744235.2018.1423703>.
44. Andrews, C.W.; Wisowaty, J.; Davis, A.O.; Crouch, R.C.; Martin, G.E. Molecular modeling, NMR spectroscopy, and conformational analysis of 3',4'-anhydrovinblastine. *J. Heterocycl. Chem.* **1995**, *32*(3), 1011-1017, <https://doi.org/10.1002/jhet.5570320357>.
45. HyperChem, version 8.0; Hypercube Inc: Gainesville, FL, USA (**2007**).
46. Sarasia, E.M.; Afsharnejad, S.; Honarparvar, B.; Mollaamin, F.; Monajjemi, M. Estrogenic active stilbene derivatives as anti-cancer agents: A DFT and QSAR study. *Phys. Chem. Liq.* **2011**, *49*, 561-571. <https://doi.org/10.1080/00319101003698992>.
47. Ghalandari, B.; Monajjemi, M.; Mollaamin, F. Theoretical Investigation of Carbon Nanotube Binding to DNA in View of Drug Delivery. *J. Comput. Theor. Nanosci* **2011**, *8*, 1212-1219, <https://doi.org/10.1166/jctn.2011.1801>.
48. Monajjemi, M.; Farahani, N.; Mollaamin, F. Thermodynamic study of solvent effects on nanostructures: Phosphatidylserine and phosphatidylinositol membranes. *Phys. Chem. Liq* **2012**, *50*, 161-172. <https://doi.org/10.1080/00319104.2010.527842>.
49. Khaleghian, M.; Zahmatkesh, M.; Mollaamin, F.; Monajjemi, M. Investigation of Solvent Effects on Armchair Single-Walled Carbon Nanotubes: A QM/MD Study. *Fuller. Nanotub. Carbon Nanostructures.*, **2011**, *19*, 251-261, <https://doi.org/10.1080/15363831003721757>.